IEEE Access
Multidisciplinary ⋮ Rapid Review ⋮ Open Access Journal

Received 2 July 2023, accepted 14 July 2023, date of publication 18 July 2023, date of current version 25 July 2023.

Digital Object Identifier 10.1109/ACCESS.2023.3296477

RESEARCH ARTICLE

A Two-Dimensional 6 × 4-Way Hollow Waveguide Beam-Switching Matrix

QI LI[1], (Graduate Student Member, IEEE), JIRO HIROKAWA[1], (Fellow, IEEE), TAKASHI TOMURA[1], (Member, IEEE), YUTA TAKAHASHI[2], NAOKI KITA[2], (Member, IEEE), AND NELSON J. G. FONSECA[3], (Senior Member, IEEE)

[1]Department of Electrical and Electronic Engineering, Tokyo Institute of Technology, Tokyo 152-8552, Japan
[2]NTT Access Network Service Systems Laboratories, Nippon Telegraph and Telephone Corporation, Yokosuka-shi 239-0847, Japan
[3]Antennas and Sub-Millimetre Waves Section, European Space Agency, NL-2200 AG Noordwijk, The Netherlands

Corresponding author: Qi Li (li.q.ag@m.titech.ac.jp)

ABSTRACT This paper presents a design of a two-dimensional (2-D) 6 × 4-way hollow waveguide beam-switching matrix working at 28.25 GHz, with a fractional bandwidth of 7.1%. It is the first time that a 2-D one-body hollow waveguide beam-switching matrix is proposed with different number of beams in two orthogonal directions. This matrix is partially adopting two-plane couplers to reduce its overall dimensions. A prototype of the complete matrix is manufactured and measured using a planar scanning near-field setup to verify the simulation results. At the center frequency of 28.25 GHz, the highest directivity is obtained for the beam having the smallest tilting angle, with a value of 21.1 dBi in simulation and 21.3 dBi in measurement. The lowest directivity corresponds to the beam having the largest tilting angle, with a simulated value of 16.0 dBi and a tilting angle of 52° from the boresight, which represents a worst-case scan loss of 5.1 dB. The measured value is overestimated in that specific case, as a consequence of the truncation in the planar near-field test setup which has higher impact on the most tilted beams. The patterns are nevertheless in good agreement and the proposed matrix is a good candidate for applications requiring a different beam distribution in two orthogonal directions.

INDEX TERMS Beam-switching matrices, hollow waveguide, two-plane coupler, 2-D beam-switching.

I. INTRODUCTION

Beam-switching circuit technology has received a great deal of attention over recent years, mainly for its increasingly wide application in massive MIMO systems and terrestrial or non-terrestrial communication systems [1], [2]. As far back as the early 1960s, when the Blass matrix [3], the Nolen matrix [4], [5] and the Butler matrix [6] were proposed, all the way till now, many investigations have been undertaken to further broaden the types and functionalities of beam-switching matrices. In 2021, [7] introduced a novel configuration of generalized one-dimensional (1-D) parallel matrix with an arbitrary number of beams, as an improvement of the parallel Nolen matrix design in [8] and resulting in a more compact configuration.

The associate editor coordinating the review of this manuscript and approving it for publication was Feng Lin.

Butler matrices are very popular among researchers because of their relatively simple design, which requires only hybrid couplers. In addition, only half of 1-D matrices need to be designed taking advantage of their symmetry. As suggested in the seminal paper by Butler and Lowe [6], 2-D beam switching can be realized by cascading 1-D beam switching matrices implemented along two directions. Similarly, the symmetries in the 2-D matrices enable to reduce the design to a quarter portion of the complete structure, as the remaining portions can be mirror-like duplicated. However, the Butler matrices in their standard form are restricted to beam numbers in the form 2^n, where n is a positive integer. The Nolen matrix, however, can have by design any number of beams. An asymmetrical N-way Nolen matrix is composed of $N(N-1)/2$ units with the couplers having several different values, leading to a complicated design process. In addition, the Nolen matrix in its original form is usually not wideband,

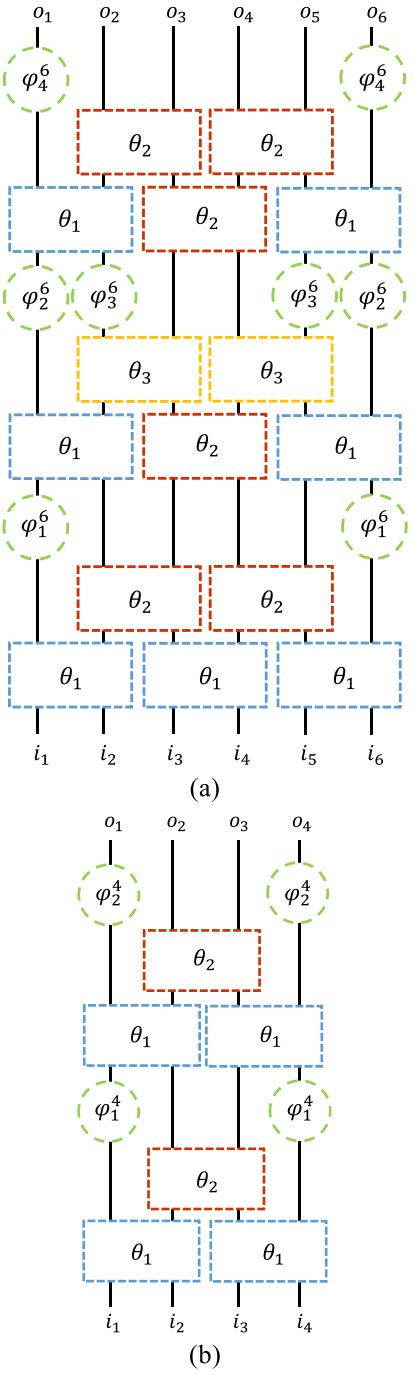

FIGURE 1. Configuration of the 1-D beam-switching matrices: (a) 6-way matrix. (b) 4-way matrix ($\theta_1 = \pi/4$, $\theta_2 = \pi/2$, $\theta_3 = arccos(1/\sqrt{3})$).

as a direct consequence of the series-fed configuration. The generalized 1-D matrix with an arbitrary number of beams introduced in [7], combines merits of both the Butler matrix and the Nolen matrix. According to the methodology in [7], a 1-D $2n$-way matrix having all $(2n)!$ permutations of the beam assignments and associated adjacent output phase differences can be obtained adjusting the values of the phase shifters. Some of the solutions from those beam assignments exhibit a symmetrical structure by adequate selection of the values of the phase shifters. This is beneficial since it reduces the design effort.

Many 1-D or 2-D beam-switching matrices are reported in the literature, using various transmission line technologies, such as microstrip line [9], [10], [11], [12], [13], [14], substrate integrated waveguide (SIW) [15], [16], [17], [18], [19], [20], [21], [22], [23], [24] and metal-wall waveguide [25], [26], [27]. For those dielectric-filled transmission lines, their loss is significant at higher frequency bands and in particular, millimeter-waves. In contrast, metal-wall waveguide, also referred to as hollow waveguide, is a transmission line technology with much reduced conductive loss [26] compared with those of dielectric planar transmission lines. The concept of the two-plane hollow waveguide coupler was first introduced in [28], and employed in a 2-D 4 × 4-way Butler matrix [26], and a 2-D 8 × 8-way Butler matrix [27]. It improves drastically the design of hollow-waveguide beam-switching matrices due to their physical miniaturization compared with the more conventional cascading of H-plane and E-plane couplers. The bandwidth of the two-plane coupler can be enhanced for the demand of specific practical applications by utilizing 2-D FEM (Finite Element Method) analysis [29] and by introducing an arbitrary shape of the coupling region [30].

This paper presents the details of a 1-D 6-way matrix and a 1-D 4-way matrix with a symmetrical structure. Based on that, the configuration of a 2-D symmetrical 6 × 4-way beam switching matrix is reported. To the best of the authors' knowledge, this is the first time that a 2-D beam-switching matrix is described having different number of beams in two orthogonal directions. This more general design enables to better adapt the number of beams and their distribution to a given application. For example, terrestrial wireless communication systems often require more beams in azimuth than in elevation angle. A prototype of the proposed 2-D 6 × 4-way-matrix is manufactured using CNC (Computer Numerical Control) milling and tested. The simulated and measured results are compared and discussed. Finally, a conclusion together with perspectives on future works are given.

II. CONFIGURATION OF THE 2-D 6×4-WAY MATRIX

A $2n$-way generalized parallel symmetrical matrix has a symmetrical port assignment,

$$p(k) = -p(2n + 1 - k) \tag{1}$$

Here p and k mean the phase difference between adjacent output ports and the input port number with incident signal, respectively. Based on the original model in [7], and by adjusting positions of some components, the employed symmetrical 1-D 6-way and 4-way matrix configurations are obtained, as shown in Fig. 1. Each quadrature coupler is identified by an angle θ_i, which defines its transmission matrix,

$$T_i = \begin{pmatrix} \cos\theta_i & -j\sin\theta_i \\ -j\sin\theta_i & \cos\theta_i \end{pmatrix} \tag{2}$$

For different port assignments of the 6-way and 4-way matrices, the coupling ratio of each quadrature coupler is fixed. By reviewing the 6-way matrix in Fig. 1(a), the structure can be a mirror-like self-duplication of 3-way Nolen matrices, by referring to [7], and the following condition is verified,

$$\varphi_3^6 = \varphi_4^6 \tag{3}$$

The values of the phase shift φ_i^6 in the proposed 6-way matrix and φ_i^4 in the 4-way matrix together with their corresponding port assignments are listed in Table 1. It is noteworthy that although all 2^n $(n!)$ permutations of symmetrical port assignments have corresponding matrix configurations [7], the 6-way and 4-way matrices with enforced symmetrical configuration have only four solutions each, reported in Table 1. Because all the quadrature couplers employed in the 6-way and 4-way matrix configurations have a transmission phase, compensating phase shifters are introduced in a practical design [8]. With regard to the 4-way matrix in Fig. 1(b), the first port assignment in Table 1(b) is equivalent to that of the conventional 4-way Butler matrix, based on the topology in this paper where we assume that all couplers, including crossovers ($\theta_2 = \pi/2$), as set in eq. (2), have a 90° phase delay in the crossing path, while all the crossovers in a Butler matrix have no phase differences between the two output ports.

As schematically represented in Fig. 2(a), the first step in the definition of the 2-D 6 × 4-way matrix consists in having 6-way matrices horizontally-placed (H-plane) and vertically-stacked (E-plane), connecting with vertically-placed and horizontally-stacked 4-way matrices. Each layer of the 6-way matrices is labelled as H_n and those of the 4-way matrices as V_n, which stands for the transmission matrix of the associated layer. The transmission of the entire cascaded 2-D 6 × 4-way matrix can be expressed as,

$$T = H_1H_2H_3H_4H_5H_6H_7H_8H_9V_1V_2V_3V_4V_5V_6 \tag{4}$$

Considering the commutativity between the vertically-stacked and horizontally-stacked layers,

$$H_iV_k = V_kH_i \tag{5}$$

Consequently, 5005 permutations can be derived adjusting the order of each layer. To properly merge phase shifter layers in the 6-way matrix and 4-way matrix, the following transmission is adopted into the design,

$$T = (H_1V_1)\,H_2V_2\,(H_3V_3)\,H_4H_5H_6H_7V_4H_8V_5\,(H_9V_6) \tag{6}$$

Fig. 2(b) gives the perspective view of the three-dimensional (3-D) inner waveguide cavities of all the components of the 2-D 6 × 4-way matrix. The center frequency of this matrix is 28.25 GHz. The layer (H_1V_1) in eq. (6) is designed using two-plane couplers, which is a hybrid coupler with the physical parameters in [30], while the remaining couplers are all designed as conventional H-plane or E-plane couplers. Note that the structure could be further simplified and miniaturized using more two-plane couplers.

TABLE 1. Port assignments with corresponding phase shifts.

(A) SIX-WAY MATRIX

$[p_1, p_2, p_3, p_4, p_5, p_6]$	φ_1^6	φ_2^6	$\varphi_3^6(\varphi_4^6)$
$\left[\frac{5\pi}{6}, \frac{-\pi}{6}, \frac{-3\pi}{6}, \frac{3\pi}{6}, \frac{\pi}{6}, \frac{-5\pi}{6}\right]$	0	$\frac{-5\pi}{6}$	$\frac{-\pi}{3}$
$\left[\frac{\pi}{6}, \frac{-5\pi}{6}, \frac{-3\pi}{6}, \frac{3\pi}{6}, \frac{5\pi}{6}, \frac{-\pi}{6}\right]$	0	$\frac{5\pi}{6}$	$\frac{\pi}{3}$
$\left[\frac{-\pi}{6}, \frac{5\pi}{6}, \frac{-3\pi}{6}, \frac{3\pi}{6}, \frac{-5\pi}{6}, \frac{\pi}{6}\right]$	π	$\frac{-5\pi}{6}$	$\frac{-\pi}{3}$
$\left[\frac{-5\pi}{6}, \frac{\pi}{6}, \frac{-3\pi}{6}, \frac{3\pi}{6}, \frac{-\pi}{6}, \frac{5\pi}{6}\right]$	π	$\frac{5\pi}{6}$	$\frac{\pi}{3}$

(B) FOUR-WAY MATRIX

$[p_1, p_2, p_3, p_4]$	φ_1^4	φ_2^4
$\left[\frac{\pi}{4}, \frac{-3\pi}{4}, \frac{3\pi}{4}, \frac{-\pi}{4}\right]$	$\frac{-\pi}{4}$	$\frac{\pi}{2}$
$\left[\frac{3\pi}{4}, \frac{-\pi}{4}, \frac{\pi}{4}, \frac{-3\pi}{4}\right]$	$\frac{\pi}{4}$	$-\frac{\pi}{2}$
$\left[\frac{-\pi}{4}, \frac{3\pi}{4}, \frac{-3\pi}{4}, \frac{\pi}{4}\right]$	$\frac{-3\pi}{4}$	$\frac{-\pi}{2}$
$\left[\frac{-3\pi}{4}, \frac{\pi}{4}, \frac{-\pi}{4}, \frac{3\pi}{4}\right]$	$\frac{3\pi}{4}$	$\frac{\pi}{2}$

However, in this specific case, some constraints related to the CNC milling process limit the design of the couplers. The frequency bandwidth of the targeted application is from 27.25 GHz to 29.25 GHz, corresponding to a 7.1% fractional bandwidth, which is difficult to achieve with the two-plane coupler having rectangular notches. Here, only the two-plane coupler of layer (H_1V_1), which is a balanced coupler in both directions, achieved the desired bandwidth with acceptable amplitude and phase variations. For further miniaturization, the two-plane coupler with an arbitrary shape of the coupled region [30] may be used to achieve the range of coupling needed while maintaining the targeted bandwidth. However, this design is generally not compatible with the CNC milling process combined with the mechanical design of the overall assembly cutting waveguides through their E-planes. This limitation of fabrication may be overcome in the future by adopting other advanced fabrication technologies, such as 3-D printing [31]. Before the layer (H_1V_1), a segment of oblique waveguides is introduced to realize a transition from the input ports to the matrix body, the size and spacing of which correspond to those of an existing 64-port coaxial-to-waveguide transformer, used for test purposes. The designed 2-D 6 × 4-way matrix only utilizes 24 ports of the transformer, while the remaining ones are left unconnected.

In this design, the Port 1 assignment for the 6-way matrix and the Port 1 assignment for the 4-way matrix in Table 1 are employed together with corresponding phase shift values. However, the phase shifters in the layers (H_3V_3), H_6 and (H_9V_6) should not only introduce the phase shift value required by design, but also compensate the transmission

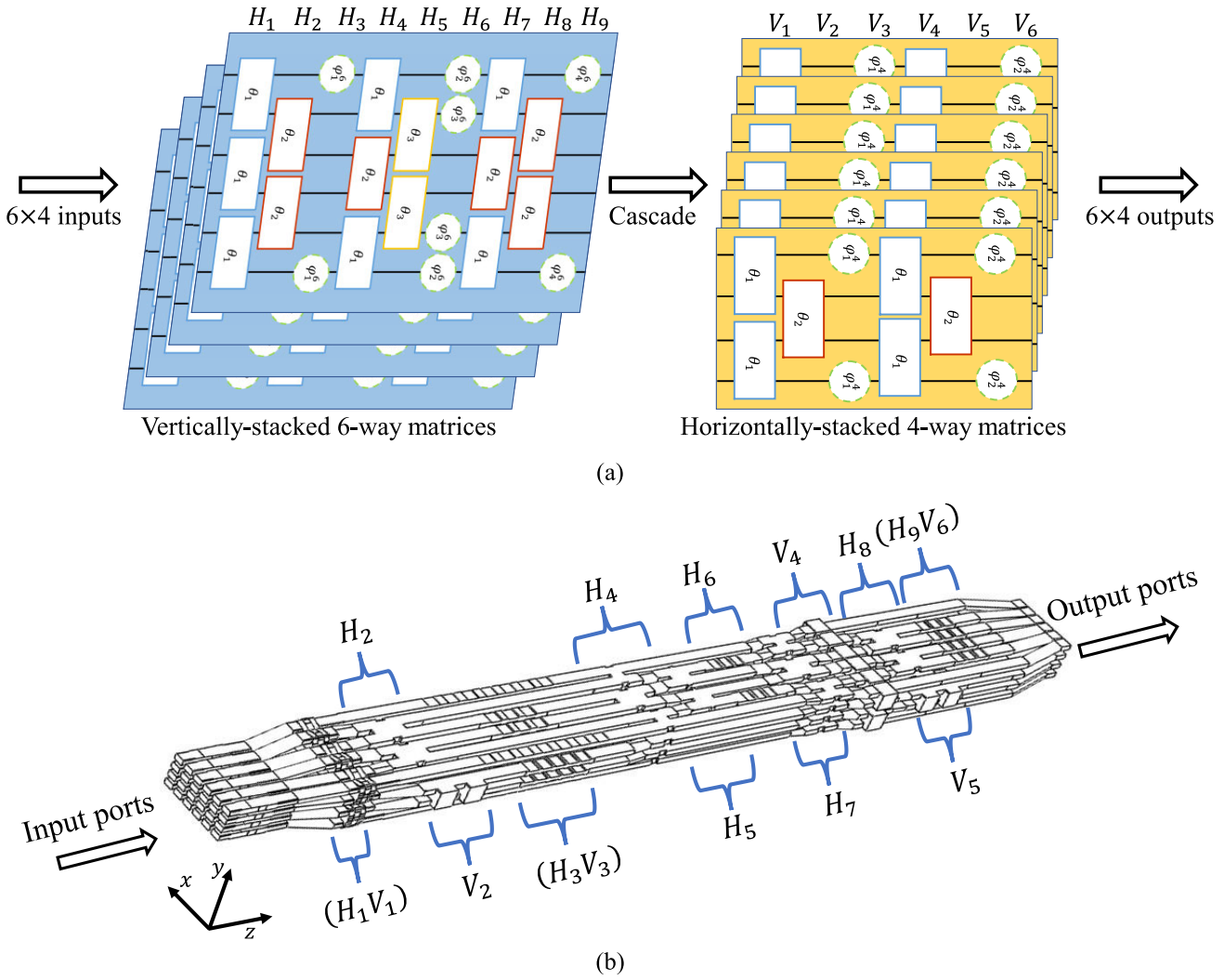

FIGURE 2. (a) Direct cascading of vertically-stacked 6-way matrices and horizontally-stacked 4-way matrices. (b) Perspective view of 3-D inner waveguide cavities of the proposed 2-D 6×4-way matrix.

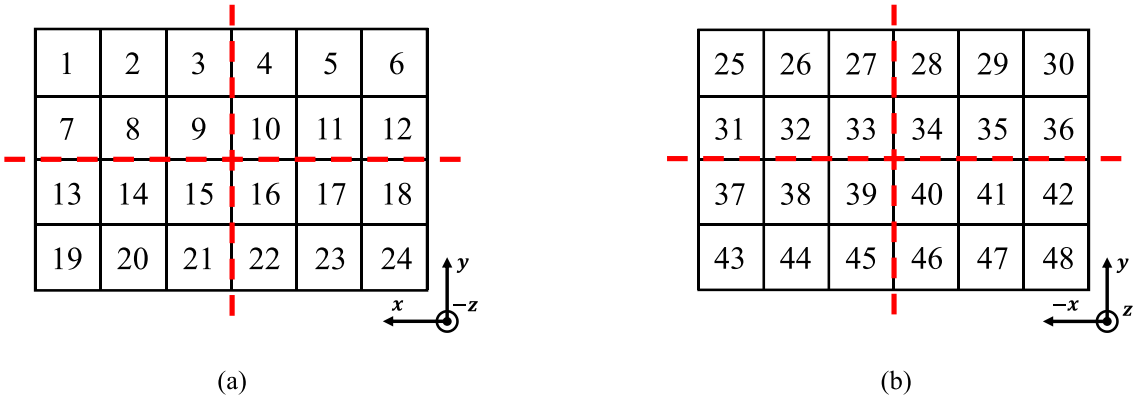

FIGURE 3. Numbering of (a) input ports and (b) output ports. Red dotted line: symmetrical axes.

phase of the couplers and oblique waveguides they are connecting with, comparing with a given reference port in each phase shifter layer.

III. PERFORMANCE OF THE 2-D 6×4-WAY MATRIX

The performance of this 2-D 6×4-way matrix is demonstrated in two steps. The first one concerns the S-parameters

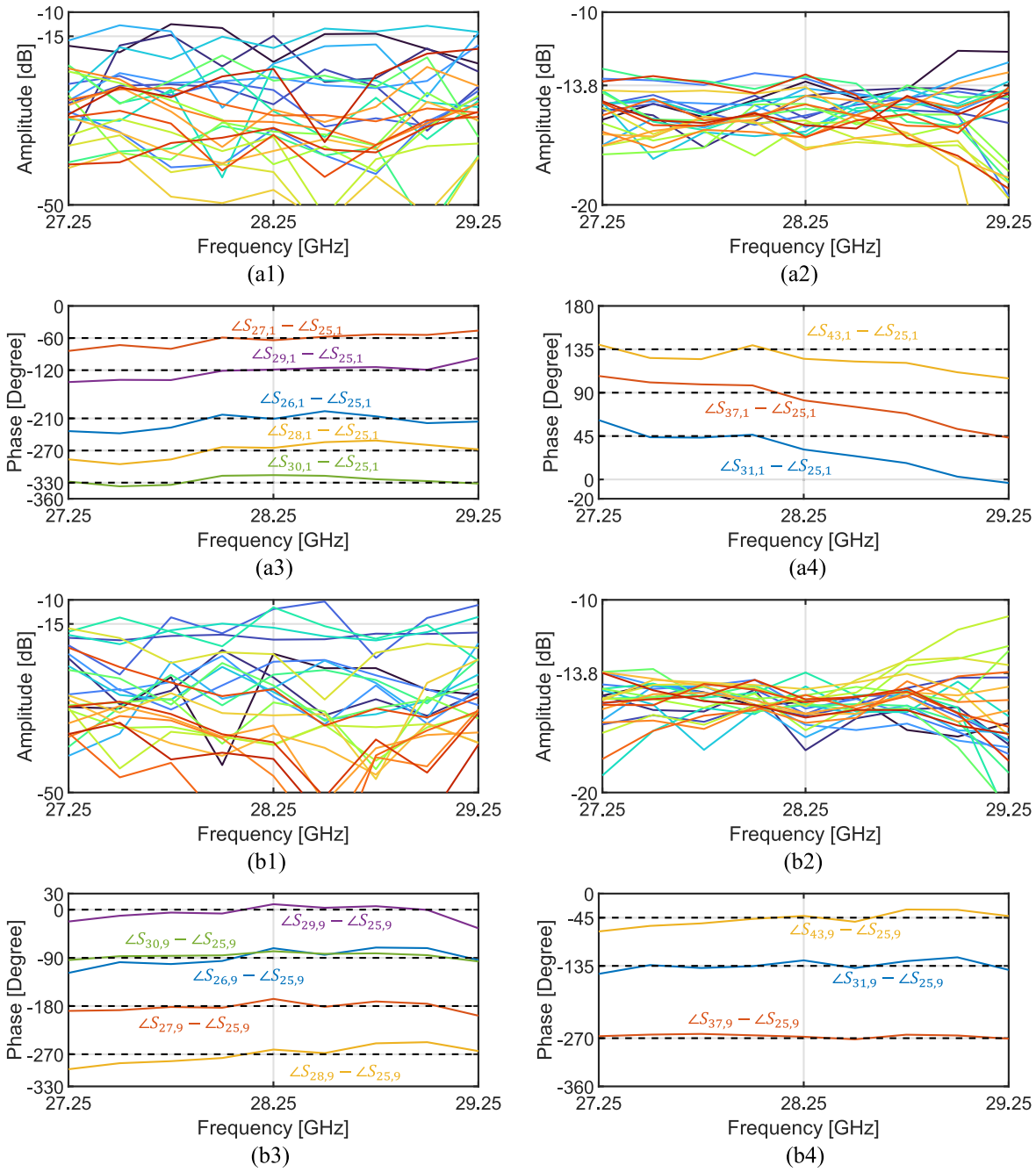

FIGURE 4. S-parameters of the 48-port network for incidence from Port 1 in terms of (a1) reflection and isolations. (a2) Output amplitudes. (a3) Phase difference with reference to Port 25 in the horizontal direction. (a4) Phase difference with reference to Port 25 in the vertical direction. For incidence from Port 9 in terms of (b1) reflection and isolations. (b2) Output amplitudes. (b3) Phase difference with reference to Port 25 in the horizontal direction. (b4) Phase difference with reference to Port 25 in the vertical direction.

of the entire 48-port network obtained in simulation, and the second one reports on the radiation of the open-ended 24-port network, in which the output ports are directly radiating into free space without loading external antennas, verified by both simulation and measurement. Note that due to the size of the matrix, a complete experimental verification is time consuming. For this reason, measurements were only performed in the most relevant configuration, corresponding to the radiating case. The numbers of the input and output ports as shown in Fig. 3, are marked from 1 to 24 and from 25 to 48, respectively. Considering the 2-D symmetry with respect to the transverse directions, the performance

of the entire matrix is fully validated investigating cases of incidence from a quarter of the input ports, such as Port 1, 2, 3, 7, 8 and 9 as defined in Fig. 3(a).

Fig. 4 provides the S-parameters of the 48-port network from 27.25 GHz to 29.25 GHz assuming incidence from Port 1 and Port 9 as examples, in terms of reflection and isolations at the input ports, output amplitudes and phase differences with reference to Port 25 of Ports 26, 27, 28, 29 and 30 in the horizontal and Ports 31, 37 and 43 in the vertical directions. From the results in Fig. 4(a1), it appears that most of the reflections and isolations are suppressed under −15 dB, with the exception of few of them with a higher level but all under −10 dB. Meanwhile, in Fig. 4(a2), the output amplitudes are nearly centering at −13.8 dB, which corresponds to the value in decibel of an identical power dividing by 24 ports. Some of the outputs have large deviations, which even go below −20 dB at some frequency points. However, considering the overall 24 ports, these few ports with higher deviation are expected to have minor influence on the uniformity of the field distribution at the output ports, and thus on the radiation performance. In Fig. 4(a3) and (a4), the phase difference with reference to Port 25 also remains stable around the ideal distribution, except for values in the vertical direction for incidence from Port 1 in the upper part of the frequency range analyzed. Interestingly, it can be noted that although the simulated values deviate from the theoretical ones, the trend is the same for all ports reported (Ports 31, 37 and 43), which indicates the deviation results from the reference Port 25 mainly. Thus, similarly to the dispersion observed on the amplitude, these larger deviations affecting only a few ports are expected to have limited influence on the overall phase distribution at the output ports, and as a consequence on the radiation performance. Considering the complexity of the complete 48-port system, the deviations in both amplitude and phase are considered acceptable, and result from a superimposition of smaller deviations introduced by each component.

Based on the S-parameters of the full model, the insertion loss and conductor loss can be estimated as additional key indicators of the performance of this 2-D 6 × 4-way matrix. The insertion loss (IL) corresponding to incidence from Port n is derived as,

$$IL_n = 1/\sum_{i=25}^{48} |S_{in}|^2 \tag{7}$$

While the conductor loss (CL) corresponding to incidence from Port n is,

$$CL_n = 1/\sum_{i=1}^{48} |S_{in}|^2 \tag{8}$$

Fig. 5 shows the insertion loss and conductor loss of the proposed 2-D 6 × 4-way matrix across the operation bandwidth. The material of the matrix is aluminum, with an electrical conductivity of 3.8×10^7 S/m assumed in the model, and the length of the entire matrix, including the transition from the input ports to the layer (H_1V_1) in Fig. 2, is about 650 mm. The numerical results indicate that the conductor

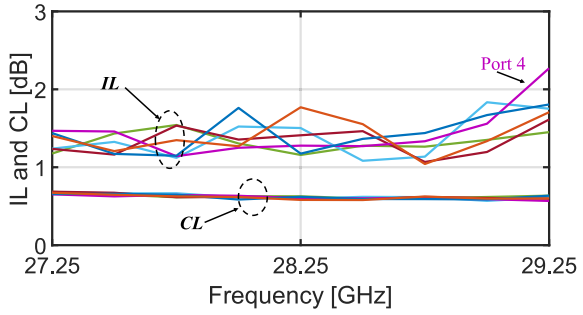

FIGURE 5. Insertion loss and conductor loss of the 2-D 6×4-way matrix.

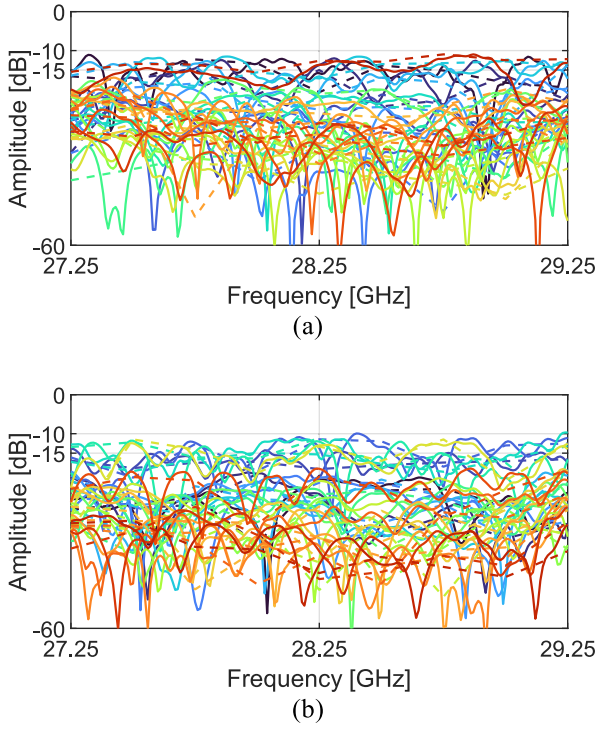

FIGURE 6. Reflection and isolation performances of the 2-D 6×4-way matrix when the output ports are directly radiating into free space for incidence from (a) Port 1. (b) Port 9. Solid line: measurement. Dotted line: simulation.

loss is stable and around 0.6 dB, which is comparable to previous works [26], [27]. The insertion loss is generally under 2 dB, except for Port 4 with values slightly larger, up to about 2.2 dB at 29.25 GHz, which remains a reasonable deviation and is also expected to have limited impact on the radiation performance.

Fig. 6 presents the reflections and isolations at the input ports when the output ports are directly radiating into free space, which are all below −10 dB. The data reported is post-processed to exclude the insertion loss of the coaxial-to-waveguide transformer. Noting that the open-ended waveguides at the output ports are 6.8 mm×3.21 mm in dimension, with the distance between adjacent ports being 7.8 mm (0.73λ) in the H-plane and 6.9 mm (0.65 λ) in the E-plane directions, it is expected that strong port-to-port coupling will

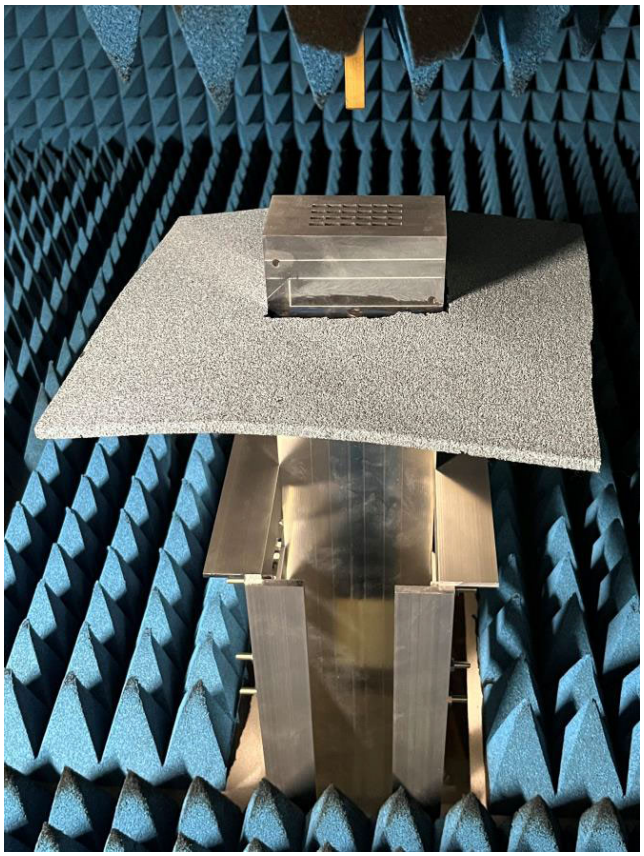

FIGURE 7. Planar scanning near field measurement setup.

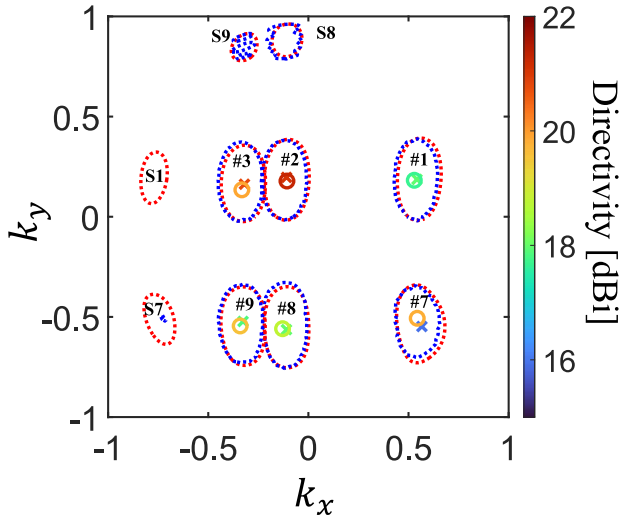

FIGURE 8. Contour plots at 3.9 dB below the peak directivity for the six tested beams of the complete 2-D 6×4-way matrix at 28.25 GHz. O: peaks in measurement. X: peaks in simulation. Blue: measurement. Red: simulation. #: main lobes. S: grating lobes.

occur and may lead to differences in reflections and isolations compared to Fig. 4(a1), (b1) where the output ports were ideally matched. The results in Fig. 6 are more representative of the actual operating performance and are suitable for the targeted applications.

TABLE 2. Directivity of each tested beam at 28.25 GHz.

Port No.	Directivity (dBi)		$[\theta, \varphi]$ (deg.)	
	Meas.	Sim.	Meas.	Sim.
1	17.7	18.0	[34, 19]	[35, 19]
2	21.3	21.1	[12, 121]	[13, 119]
3	19.9	20.8	[21, 158]	[21, 153]
7	19.8	16.0	[-48, 137]	[-52, 136]
8	18.8	18.0	[-35, 77]	[-35, 79]
9	19.6	17.9	[-40, 58]	[-38, 58]

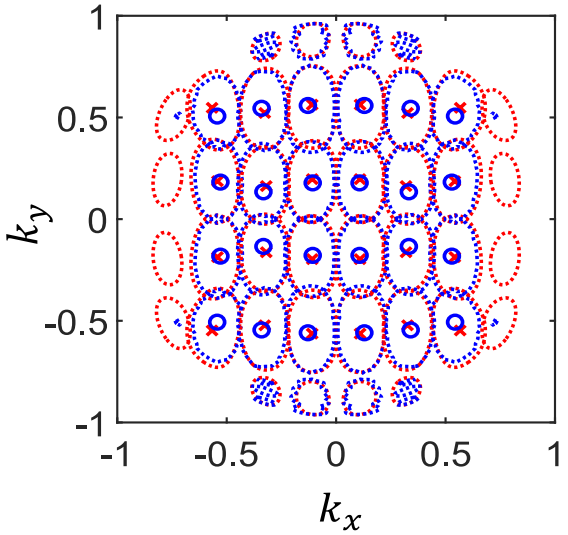

FIGURE 9. Contour plots at 3.9 dB below the peak directivity of all the beams of the complete 2-D 6×4-way matrix at 28.25 GHz. O: peaks in measurement by mirror-like duplication of the six tested beams. X: peaks in simulation. Blue: measurement. Red: simulation.

The radiation performance is verified using planar scanning near-field measurements. Fig. 7 depicts the test setup of the planar scanning near-field measurements when the 2-D 6 × 4-way matrix is loaded in the chamber surrounded by absorbers. Some fixtures are utilized to support the matrix body. The probe position is 54.0 mm above the aperture, and the scanning range is a square area of size 660mm × 660mm, corresponding to an 80.7° angle tilting from the zenith. The resulting truncation effect, due to the radiated energy not captured in the scanning area, is a known limitation of planar scanning near-field measurements. This usually has a limited impact on the beams closer to zenith, while larger deviations are expected for the most tilted beams.

Fig. 8 displays the contour plots at −3.9 dB below the peak directivity of each beam at the center frequency of 28.25 GHz. The peak values as well as directions in elevation

and azimuth are listed in Table 2. The definitions of k_x and k_y are $\sin\theta\cos\varphi$ and $\sin\theta\sin\varphi$, respectively, where θ and φ are spherical coordinate angles. From Fig. 8, the contour of the main lobe for each beam agrees very well. This is also reflected in the values in Table 2, where the angular deviation in elevation or azimuth between measurement and simulation never exceeds 5°. Beams 1 and 7 are accompanied with grating lobes in the k_x direction while Beams 8 and 9 generate grating lobes in the k_y direction. However, the grating lobes of Beams 1 and 7 are almost not visible at −3.9 dB levels in measurement. The directivity values of Beams 1, 2, 3 and 8 are in good agreement for simulation and measurement data, with no more than 0.9 dB discrepancy. Beam 9 gives a slightly worse deviation of 1.7 dB. However, Beam 7 has the largest discrepancy of up to 3.8 dB. The discrepancy of the measured results away from the simulated results, including a higher directivity of the main lobes and a reduced level of the side lobes, mainly comes from the lower accuracy of the planar scanning near-field measurement for large angle tilted beams resulting from the truncation effect discussed above, as Beam 7 corresponds to the phase difference in the H-plane of $5\pi/6$ and in the E-plane of $-3\pi/4$, both of which stand for the largest phase differences in either directions of the matrix, as well as a largest tilted angle of 52° with reference to the boresight direction. Considering the symmetry of beams, the full 24 beams contour map are provided in Fig. 9 by mirror-like duplication of the six tested beams.

The radiation patterns at the center frequency are given in Fig. 10 for each measured beam, fixing k_x such to cut through the peak direction and scanning along the k_y direction, or alternatively fixing k_y such to cut through the peak direction and scanning along the k_x direction. The beam shapes in measurement are consistent with those in simulation. From Fig. 10(a)(c), it can be noticed that the sidelobe levels of Beams 1 and 7 in measurement are lower than those in simulation, leading to sidelobe contours in Fig. 8 disappearing.

Table 3 provides a detailed comparison of this work with other related works, particularly putting emphasis on the comparison of waveguide-type matrices to show the difference on performance as a function of the numbers of beams. This works reports on the first 2-D hollow-waveguide beam-switching matrix with different number of beams in two orthogonal directions, which is the main differentiating factor compared to all previously reported works of Table 3. The design in this paper does make use of two-plane couplers. However, as explained in Section II, the bandwidth requirements combined with some fabrication technology limitations constrained their use to the hybrid couplers only, corresponding also to the type of couplers used in previous works. Compared with the 2-D 4 × 4-way Butler matrix in [26] and the 2-D 8 × 8-way Butler matrix in [27], the proposed 2-D 6 × 4-way matrix has intermediate insertion loss, which is in line with the corresponding number of ports as well as the overall network complexity. The length of this 2-D 6 × 4-way matrix, particularly in the longitudinal direction, is greater than that of the 2-D 8 × 8-way Butler matrix in [27], which is a consequence of use of conventional H-plane and E-plane couplers, based on fabrication consideration. Extending the use of two-plane couplers in

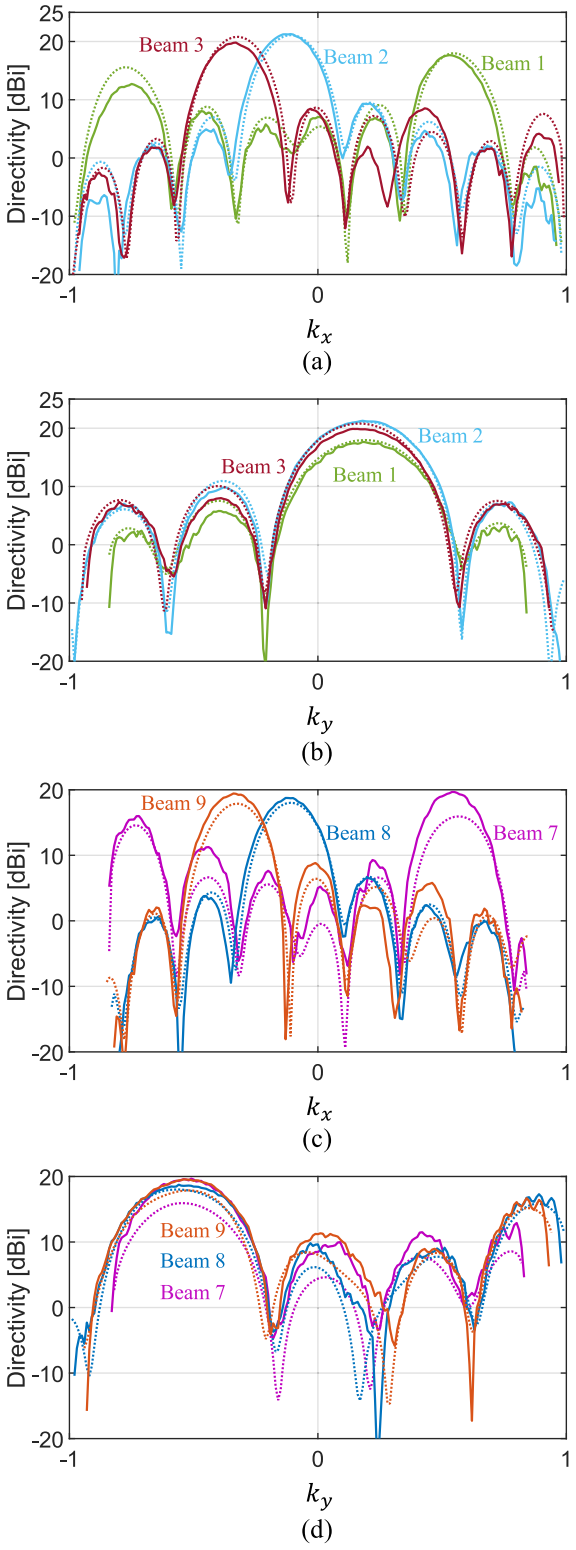

FIGURE 10. Radiation patterns at 28.25 GHz of Beams 1, 2 and 3 in (a) k_x-plane. (b) k_y-plane. Beams 7, 8 and 9 in (c) k_x-plane. (d) k_y-plane.

TABLE 3. Comparison with related works on 2-D switching matrices.

Matrix size	2-D 4×4 [13]	2-D 4×4 [23]	2-D 4×4 [26]	2-D 8×8 [27]	2-D 6×4 This work
Frequency	2.4 GHz	10.0 GHz	22.0 GHz	19.5 GHz	28.0 GHz
Technology	Microstrip line	SIW	Waveguide	Waveguide	Waveguide
Number of ports	16	16	16	64	24
One-body structure	No	No	Yes	Yes	Yes
Use of two-plane couplers	No	No	Yes	Yes	Yes
Worst-case insertion loss (IL)	1.8 dB	4.0 dB	1.5 dB	5.0 dB	2.2 dB
Bandwidth	16.7 %	N.A.	2.0 %	5.1 %	7.1 %
Physical size (λ^3)	$1.6 \times 1.6 \times 0.004$	$22.0 \times 16.7 \times 0.03$	$3.5 \times 3.5 \times 14.0$	$5.8 \times 5.0 \times 26.5$	$8.5 \times 4.3 \times 50.6$

the proposed design would bring higher integration at the expense of a reduced frequency bandwidth unless alternative manufacturing techniques are considered.

IV. CONCLUSION

This paper has introduced a 2-D hollow waveguide 6×4-way beam switching matrix working from 27.25 GHz to 29.25 GHz, with a 7.1% fractional bandwidth. This is the first time that a 2-D waveguide beam-switching matrix is proposed with different number of beams in two orthogonal directions. Taking advantage of the 2-D symmetry in the transverse directions, the design complexity is significantly reduced. The 2-D 6×4-way matrix has at most 2.2 dB insertion loss over the operation bandwidth. The radiation performance is verified by planar scanning near-field measurements. The maximum directivity is obtained for Beam 2 with a value of 21.3 dBi in measurement and 21.1 dBi in simulation. The minimum directivity in measurement is 17.7 dBi corresponding to Beam 1, with a tilted angle of 34° with reference to boresight, corresponding to a scan loss of 3.4 dB. The minimum directivity in simulation is 16.0 dBi, obtained for Beam 7 at an angle of 52° with reference to the boresight, corresponding to 5.1 dB scan loss, which has the largest discrepancy between measurement and simulation, with the measured results of 19.8 dBi in directivity, 1.5 dB in scan loss and 48° tilted angle referring to the boresight.

This 2-D 6×4-way matrix may be improved in future works exploring alternative and advanced manufacturing technologies, such as 3-D printing [31], to enable further physical miniaturization and complexity reduction by employing more two-plane couplers to replace the conventional H-plane and E-plane couplers.

REFERENCES

[1] H. Papadopoulos, C. Wang, O. Bursalioglu, X. Hou, and Y. Kishiyama, "Massive MIMO technologies and challenges towards 5G," *IEICE Trans. Commun.*, vol. E99.B, no. 3, pp. 602–621, 2016.

[2] Y. J. Guo, M. Ansari, and N. J. G. Fonseca, "Circuit type multiple beamforming networks for antenna arrays in 5G and 6G terrestrial and non-terrestrial networks," *IEEE J. Microw.*, vol. 1, no. 3, pp. 704–722, Jul. 2021.

[3] J. Blass, "Multidirectionnal antenna—A new approach to stacked beams," in *Proc. IRE Int. Conf. Rec.*, vol. 8, 1960, pp. 48–50.

[4] J. Nolen, "Synthesis of multiple beam networks for arbitrary illuminations," Ph.D. dissertation, Bendix Corp., Radio Division, Baltimore, MD, USA, Apr. 1965.

[5] N. J. G. Fonseca, "Printed S-band 4 × 4 Nolen matrix for multiple beam antenna applications," *IEEE Trans. Antennas Propag.*, vol. 57, no. 6, pp. 1673–1678, Jun. 2009.

[6] J. Butler and R. Lowe, "Beam-forming matrix simplifies design of electronically scanned antennas," *Electron. Des.*, vol. 9, pp. 170–173, Apr. 1961.

[7] J. Hirokawa and N. J. G. Fonseca, "Generalized one-dimensional parallel switching matrices with an arbitrary number of beams," *IEEE J. Microw.*, vol. 1, no. 4, pp. 975–988, Oct. 2021.

[8] T. Djerafi, N. J. G. Fonseca, and K. Wu, "Broadband substrate integrated waveguide 4 × 4 Nolen matrix based on coupler delay compensation," *IEEE Trans. Microw. Theory Techn.*, vol. 59, no. 7, pp. 1740–1745, Jul. 2011.

[9] C.-W. Wang, T.-G. Ma, and C.-F. Yang, "A new planar artificial transmission line and its applications to a miniaturized Butler matrix," *IEEE Trans. Microw. Theory Techn.*, vol. 55, no. 12, pp. 2792–2801, Dec. 2007.

[10] C. A. Guo, Y. J. Guo, H. Zhu, W. Ni, and J. Yuan, "Optimization of multibeam antennas employing generalized joined coupler matrix," *IEEE Trans. Antennas Propag.*, vol. 71, no. 1, pp. 215–224, Jan. 2023.

[11] M. Bona, L. Manholm, J. P. Starski, and B. Svensson, "Low-loss compact Butler matrix for a microstrip antenna," *IEEE Trans. Microw. Theory Techn.*, vol. 50, no. 9, pp. 2069–2075, Sep. 2002.

[12] H. Ren, H. Zhang, Y. Jin, Y. Gu, and B. Arigong, "A novel 2-D 3 × 3 Nolen matrix for 2-D beamforming applications," *IEEE Trans. Microw. Theory Techn.*, vol. 67, no. 11, pp. 4622–4631, Nov. 2019.

[13] K. Ding and A. A. Kishk, "2-D Butler matrix and phase-shifter group," *IEEE Trans. Microw. Theory Techn.*, vol. 66, no. 12, pp. 5554–5562, Dec. 2018.

[14] W. F. Moulder, W. Khalil, and J. L. Volakis, "60-GHz two-dimensionally scanning array employing wideband planar switched beam network," *IEEE Antennas Wireless Propag. Lett.*, vol. 9, pp. 818–821, 2010.

[15] A. A. M. Ali, N. J. G. Fonseca, F. Coccetti, and H. Aubert, "Design and implementation of two-layer compact wideband Butler matrices in SIW technology for Ku-band applications," *IEEE Trans. Antennas Propag.*, vol. 59, no. 2, pp. 503–512, Feb. 2011.

[16] T. Djerafi and K. Wu, "A low-cost wideband 77-GHz planar Butler matrix in SIW technology," *IEEE Trans. Antennas Propag.*, vol. 60, no. 10, pp. 4949–4954, Oct. 2012.

[17] T. Djerafi, N. J. G. Fonseca, and K. Wu, "Planar *Ku*-band 4 × 4 Nolen matrix in SIW technology," *IEEE Trans. Microw. Theory Techn.*, vol. 58, no. 2, pp. 259–266, Feb. 2010.
[18] E. T. Der, T. R. Jones, and M. Daneshmand, "Miniaturized 4 × 4 Butler matrix and tunable phase shifter using ridged half-mode substrate integrated waveguide," *IEEE Trans. Microw. Theory Techn.*, vol. 68, no. 8, pp. 3379–3388, Aug. 2020.
[19] Q. Sun, Y.-L. Ban, Y.-X. Che, and Z. Nie, "Coexistence-mode CRLH SIW transmission line and its application for longitudinal miniaturized Butler matrix and multibeam array antenna," *IEEE Trans. Antennas Propag.*, vol. 69, no. 11, pp. 7593–7603, Nov. 2021.
[20] J.-W. Lian, X.-Y. Zhao, Y.-L. Ban, Y. Liu, and Z. Nie, "Compact SIW 2-D Butler matrix and its multibeam application," *IEEE Antennas Wireless Propag. Lett.*, vol. 20, no. 3, pp. 386–390, Mar. 2021.
[21] K. Wu, M. Bozzi, and N. J. G. Fonseca, "Substrate integrated transmission lines: Review and applications," *IEEE J. Microw.*, vol. 1, no. 1, pp. 345–363, Jan. 2021.
[22] I. M. Mohamed and A.-R. Sebak, "60 GHz 2-D scanning multibeam cavity-backed patch array fed by compact SIW beamforming network for 5G applications," *IEEE Trans. Antennas Propag.*, vol. 67, no. 4, pp. 2320–2331, Apr. 2019.
[23] J.-W. Lian, Y.-L. Ban, H. Zhu, and Y. J. Guo, "Uniplanar beam-forming network employing eight-port hybrid couplers and crossovers for 2-D multibeam array antennas," *IEEE Trans. Microw. Theory Techn.*, vol. 68, no. 11, pp. 4706–4718, Nov. 2020.
[24] J.-W. Lian, Y.-L. Ban, J.-Q. Zhu, K. Kang, and Z. Nie, "Compact 2-D scanning multibeam array utilizing the SIW three-way couplers at 28 GHz," *IEEE Antennas Wireless Propag. Lett.*, vol. 17, no. 10, pp. 1915–1919, Oct. 2018.
[25] S. Yamamoto, J. Hirokawa, and M. Ando, "A single-layer hollow waveguide 8-way Butler matrix," *IEICE Trans. Electron.*, vol. 89, no. 7, pp. 1080–1088, Jul. 2006.
[26] D.-H. Kim, J. Hirokawa, and M. Ando, "One-body 2-D beam-switching Butler matrix with waveguide short-slot 2-plane couplers," *IEICE Trans. Electron.*, vol. E100.C, no. 10, pp. 884–892, 2017.
[27] T. Tomura, D.-H. Kim, M. Wakasa, Y. Sunaguchi, J. Hirokawa, and K. Nishimori, "A 20-GHz-band 64 × 64 hollow waveguide two-dimensional Butler matrix," *IEEE Access*, vol. 7, pp. 164080–164088, 2019.
[28] D.-H. Kim, J. Hirokawa, and M. Ando, "Design of waveguide short-slot two-plane couplers for one-body 2-D beam-switching Butler matrix application," *IEEE Trans. Microw. Theory Techn.*, vol. 64, no. 3, pp. 776–784, Mar. 2016.
[29] M. Wakasa, D.-H. Kim, T. Tomura, and J. Hirokawa, "Wideband design of a short-slot 2-plane coupler by the mode matching/FEM hybrid analysis considering the structural symmetry," *IEICE Trans. Commun.*, vol. E102.B, no. 5, pp. 1019–1026, May 2019.
[30] S. Chen, T. Tomura, J. Hirokawa, K. Ito, M. Suga, Y. Shirato, D. Uchida, and N. Kita, "Design for operation in two frequency bands by division of the coupled region in a waveguide 2-Plane coupler," *IEICE Trans. Electron.*, vol. E105.C, no. 12, pp. 729–739, Dec. 2022.
[31] O. A. Peverini, M. Lumia, G. Addamo, G. Virone, and N. J. G. Fonseca, "How 3D-printing is changing RF front-end design for space applications," *IEEE J. Microw.*, vol. 3, no. 2, pp. 800–814, Apr. 2023.

QI LI (Graduate Student Member, IEEE) was born in Hunan, China, in 1996. He received the B.S. degree in electrical and electronic engineering from the University of Electronic Science and Technology of China (UESTC), in 2018, and the M.S. degree in electrical and electronic engineering from the Tokyo Institute of Technology, in 2020, where he is currently pursuing the Ph.D. degree in electrical and electronic engineering.

His research interests include beam-switching waveguide circuits and waveguide slot antenna.

JIRO HIROKAWA (Fellow, IEEE) was born in Tokyo, Japan, in 1965. He received the B.S., M.S., and D.E. degrees in electrical and electronic engineering from the Tokyo Institute of Technology (Tokyo Tech), Tokyo, in 1988, 1990, and 1994, respectively.

He was a Research Associate and an Associate Professor with Tokyo Tech, from 1990 to 1996 and from 1996 to 2015, respectively, where he is currently a Professor. He was with the Antenna Group, Chalmers University of Technology, Gothenburg, Sweden, as a Postdoctoral Fellow, from 1994 to 1995. He has authored or coauthored more than 200 peer-reviewed journal articles and more than 600 international conference presentations. His research interests include analyses, designs, and fabrication techniques of slotted waveguide array antennas, millimeter-wave, terahertz antennas, and beam-switching circuits.

Dr. Hirokawa is a Fellow of IEICE. He received the IEEE AP-S Tokyo Chapter Young Engineer Award, in 1991; the Young Engineer Award from IEICE, in 1996; the Tokyo Tech Award for Challenging Research, in 2003; the Young Scientists' Prize from the Minister of Education, Cultures, Sports, Science and Technology, Japan, in 2005; the Best Paper Award, in 2007; the Best Letter Award from the IEICE Communications Society, in 2009; and the IEICE Best Paper Award, in 2016 and 2018. He was the Chair of the Technical Program Committee for ISAP 2016. He was the Chair of the IEICE Technical Committee on Antennas and Propagation, from 2017 to 2019. He served as an Associate Editor for *IEICE Transactions on Communications*, from 1999 to 2003 and from 2004 to 2007. He served as an Associate Editor and a Track Editor for IEEE TRANSACTIONS ON ANTENNAS AND PROPAGATIONS, from 2013 to 2016 and from 2016 to 2022, respectively. He has been serving as a Track Editor for IEEE ANTENNAS AND WIRELESS PROPAGATION LETTERS, since 2023.

TAKASHI TOMURA (Member, IEEE) received the B.S., M.S., and D.E. degrees in electrical and electronic engineering from the Tokyo Institute of Technology, Tokyo, Japan, in 2008, 2011, and 2014, respectively.

From 2014 to 2017, he was with Mitsubishi Electric Corporation, Tokyo, where he was engaged in research and development of aperture antennas for satellite communications and radar systems. From 2017 to 2019, he was a Specially Appointed Assistant Professor with the Tokyo Institute of Technology, where he is currently an Assistant Professor. His research interests include electromagnetic analysis, aperture antennas, and planar waveguide slot array antennas. He was a Research Fellow of the Japan Society for the Promotion of Science (JSPS), in 2013. He is a member of IEICE. He received the Best Student Award from Ericsson Japan, in 2012, the IEEE AP-S Tokyo Chapter Young Engineer Award, in 2015, and the Young Researcher Award from the IEICE Technical Committee on Antennas and Propagation, in 2018.

YUTA TAKAHASHI received the B.E. degree in electrical engineering and the M.E. and Ph.D. degrees in electrical engineering and computer science from Iwate University, Morioka, Japan, in 2012, 2014, and 2020, respectively. He joined NTT DOCOMO, in 2014, where he was engaged in research on fifth generation mobile communications system. Since 2021, he has been engaged in research on radio-over-fiber systems with NTT Access Network Service Systems Laboratories. He is a member of IEICE. He received the APMC 2014 Prize, in 2014.

NAOKI KITA (Member, IEEE) received the B.E. degree from the Tokyo Metropolitan Institute of Technology, Tokyo, Japan, in 1994, and the M.E. and Ph.D. degrees from the Tokyo Institute of Technology, Tokyo, in 1996 and 2007, respectively. In 1996, he joined NTT, where he was engaged in the research of radio wave propagation characteristics for wireless access systems, the development of future satellite communication systems, and international standardization on radio wave propagation. From 2009 to 2010, he was a Visiting Scholar with Stanford University, Stanford, CA, USA. From 2013 to 2014, he was a Visiting Research Scholar with Waseda University, Tokyo. He is currently a Senior Research Engineer, a Supervisor, and the Group Leader with NTT Access Network Service Systems Laboratories, where he engages in the research and development of future wireless access network systems. He is a Senior Member of IEICE. He received the IEICE Young Researcher's Award, the IEICE Communications Society Best Paper Award, and the IEICE Best Paper Award, in 2002, 2010, and 2014, respectively, and the Best Paper Award from the International Symposium on Antennas and Propagation 2016 (ISAP2016), in 2016.

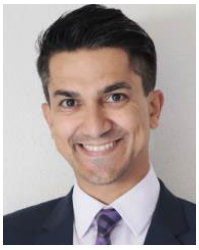

NELSON J. G. FONSECA (Senior Member, IEEE) received the M.Eng. degree in electrical engineering from Ecole Nationale Supérieure d'Electrotechnique, Electronique, Informatique, Hydraulique et Télécommunications (ENSEEIHT), Toulouse, France, in 2003, the M.Sc. degree in electrical engineering from Ecole Polytechnique de Montreal, Quebec, Canada, in 2003, and the Ph.D. degree in electrical engineering from Institut National Polytechnique de Toulouse–Université de Toulouse, France, in 2010.

He is currently an Antenna Engineer with the Antenna and Sub-Millimetre Waves Section, European Space Agency (ESA), Noordwijk, The Netherlands. Since November 2020, he has been holding an Honorary Appointment, as a Professional Fellow of the University of Technology Sydney (UTS), Ultimo, NSW, Australia. He has been a Board Member of the European School of Antennas (ESoA), since January 2019. He is actively involved as a Lecturer and a Coordinator in courses related to space and ground antennas. He has authored or coauthored more than 300 papers in peer-reviewed journals and conferences and has more than 50 patents issued or pending. His research interests include multiple beam antennas for space missions, beam-former theory and design, ground terminal antennas, and novel manufacturing techniques.

Dr. Fonseca is serving as the Chair for the Newly Founded IEEE MTT-S Technical Committee 29 on Microwave Aerospace Systems. He is the elected EurAAP Regional Delegate representing Benelux, from 2021 to 2023. He was an Associate Editor of IEEE TRANSACTIONS ON MICROWAVE THEORY AND TECHNIQUES, from 2020 to 2022, and a Guest Editor of two Focused Issues on Aerospace Applications for the *IEEE Microwave Magazine*, in 2022 and 2023. He is serving as an Associate Editor for IEEE TRANSACTIONS ON ANTENNAS AND PROPAGATION and *IET Microwaves, Antennas and Propagations*, and a Topic Editor for IEEE JOURNAL OF MICROWAVES.